

MIT OpenCourseWare  
<http://ocw.mit.edu>

8.13-14 Experimental Physics I & II "Junior Lab"  
Fall 2007 - Spring 2008

For information about citing these materials or our Terms of Use, visit: <http://ocw.mit.edu/terms>.

# Neutron Physics

MIT Department of Physics  
(Dated: August 1, 2005)

The Maxwell-Boltzmann distribution and Bragg scattering of thermalized neutrons; the DeBroglie relation; neutron absorption cross sections. The technique of time-of-flight spectroscopy with a mechanical beam chopper is used to study the properties of thermal neutrons in a beam emerging from the MIT research reactor. First, the distribution in velocity of the neutrons is measured, and the results are compared with the Maxwell Boltzmann distribution for the temperature of the reactor. Second, the DeBroglie relation between wavelength and momentum of neutrons is determined from measurements of the angle of Bragg reflection of the beam from a copper crystal as a function of the velocity measured by time-of-flight. Third, the absorption cross sections of several elements are measured, and the  $1/v$  dependence of the boron cross section is observed.

## PREPARATORY QUESTIONS

1. Compute the average velocity,  $\sqrt{\langle v^2 \rangle}$ , of neutrons in a beam emerging from a reactor operating at  $50^\circ\text{C}$ .
2. Describe how a proportional counter containing boron trifluoride ( $\text{BF}_3$ ) works to detect neutrons. Why is a low efficiency detector used for the measurement of the velocity distribution of the thermal neutrons?
3. Compute the angles of first order Bragg diffraction of 0.025 eV neutrons from the (200) and (111) planes of crystalline copper. Could you diffract 0.0025 eV neutrons from a copper crystal?
4. Suppose a measurement shows that a sheet of linear thickness  $x$  of a particular element of atomic weight  $A$  and density  $\rho$  reduces the intensity of a beam of monoenergetic neutrons by the ratio  $I/I_0$ . Derive a formula for the cross section  $\sigma$  of the element for absorption of neutrons in terms of these defined quantities.

## 1. SUGGESTED PROGRESS CHECK FOR END OF 2ND SESSION

Using MCS distributions of neutron time of flights at the near and far detector positions, calculate the velocity of the particles to zeroth order.

## 2. EXPERIMENTATION AT THE MIT RESEARCH REACTOR (MITR): RADIATION PROTECTION AND SECURITY

This experiment was developed for Junior Lab by Professor Clifford Shull [1]. It employs a rather intense beam of low energy neutrons produced at the MIT Research Reactor located in Building NW12 on the edge of the campus at 138 Albany Street. The MIT reactor has been operating for 30 years and has served as a base for countless investigations by faculty, graduate and undergraduate thesis students, and UROP and other undergraduate

student projects. Use of its facilities is perfectly safe, providing reasonable and common-sense guidelines and procedures are followed. To insure that you are familiar with these procedures, a certain amount of indoctrination is required. This involves some advance study of material, followed by a briefing by staff from the Radiation Protection Office and from the Reactor Operations Group. Following completion of this procedure, you are “cleared” to perform the experiment on your own initiative and according to your own schedule, consistent with that of other students and the operation schedule of the facility. In keeping with the spirit of the Junior Lab, you will operate all the equipment yourself, although members of the teaching staff will generally be available to explain details and answer questions, particularly during your first session.

Access to the reactor building is restricted in keeping with regulations at this and every other nuclear reactor facility in this country (or anywhere for that matter). You cannot come and go until you have been granted “clearance”. Federal and state government regulations specify how this is to be obtained. For the purpose of Junior Laboratory experimentation, the following steps should be taken in order:

1. Download the web-based training instructions from <http://web.mit.edu/8.13/www/38.shtml>. Follow these instructions to successfully complete your General Employee Radiological Training (GERT). Altogether this will take about two hours, and can be done at home.
2. After completing your GERT, you must attend a scheduled briefing session (normally held on the 2nd and 3rd Fridays of the fall term) at the reactor to discuss the material and to complete any required forms. Following this discussion, you will be taken on an Inspection Tour of the reactor by the operating staff. The discussion period and tour will take about 1.5 hours—thereafter you will be immediately “cleared”, and able to get on with the experiment. You will notice that entry into the reactor building is through a locked gate which may be opened with a magnetically-coded identification card, issued to you upon your clearance.

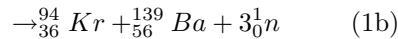
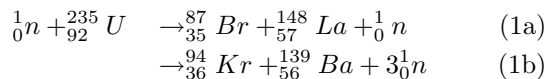
The equipment is reserved for your use at the scheduled time. You may also use it at other times, such as evenings, Fridays and weekends. If you wish to use the facility outside of your normally scheduled time, please first consult Judith Maro, Irradiation Services Coordinator at “jmaro@mit.edu” prior to going to the reactor. You should also clear any proposed changes to your scheduled attendance with your Section Instructor.

3. During your first scheduled period, Dr. Sewell (ext 3-5082) or a TA will be present to show you the apparatus and procedures. Please contact Dr. Sewell in advance if a conflict or change of schedule interferes with this important introductory session.

### 3. OPERATIONAL PHYSICS OF THE NUCLEAR REACTOR

The nuclear reactor is a chain-reacting system which bears resemblance in operational principle to a coal fire, with nuclear reactions being the source of heat rather than chemical reactions. In a coal fire, some carbon atoms are excited by thermal “starting” so that they combine with oxygen (burn). The heat released in this exothermic chemical reaction activates other carbon atoms to do the same, thereby forming a chain reaction without further need of “starting”. The fire grows in intensity until an equilibrium level is reached, wherein heat losses from the system limit the thermal power available for further steps in the chain reacting process.

In a nuclear reactor, the counterpart to the carbon fuel is the nuclear fuel (most commonly the fissionable isotope of uranium,  $^{235}_{92}\text{U}$ ), and neutrons serve as the communicative thermal energy counterpart. In 1939 Hahn and Strassman discovered that neutrons react with uranium nuclei to cause fission in which the heavy nucleus splits into two smaller and not necessarily equal nuclei plus “debris” such as neutrons, gamma-rays, electrons, etc. The fragmentation can proceed in many different ways. Typical reactions are shown in Equation 1.



Notice that the above reaction equations are written as balanced equations in both numbers of nucleons and charge. However, if you look in a table of precise mass values, you will find for the nuclear masses of the entries in the first reaction the values:

$$M({}^{235}_{92}\text{U}) = 235.11240$$

$$M({}^{87}_{35}\text{Br}) = 86.95722$$

$$M({}^{148}_{57}\text{La}) = 147.98930$$

These values imply a mass loss of 0.16588 mass units in the reaction. Using the Einstein mass-energy equivalence, this calculates to 155 MeV of energy which, according to the energy conservation principle, must show up as

kinetic energy distributed among the reaction fragments. This is a very large amount of energy when compared with that of ordinary nuclear processes such as alpha, beta or gamma decay (1–10 MeV), and especially when compared to chemical reactions ( $\sim 5$  eV).

A second notable feature of fission reactions is that neutrons are released as debris. Shortly after the discovery of fission careful measurements in several laboratories proved that the average number of neutrons released per fission is more than one. It was then apparent that under appropriate circumstances these neutrons could initiate fission of other  $^{235}_{92}\text{U}$  nuclei and that the physical basis for a nuclear chain reaction exists. The possibilities for practical nuclear power generation and bombs were immediately recognized by experts all over the world, and a race began. The first controlled nuclear chain reaction was achieved in 1941 at the University of Chicago by a team under the direction of Enrico Fermi, and the first bomb was exploded in 1945.

Nuclide	$\nu$ , Per Thermal N Induced Fission	$\eta$ , Per Thermal N Absorbed	$\eta$ , Per Fast N Absorbed
$^{233}_{92}\text{U}$	2.50	2.27	2.60
$^{235}_{92}\text{U}$	2.43	2.06	2.18
$^{239}_{94}\text{Pu}$	2.90	2.10	2.74

TABLE I: Number of Neutrons Liberated per Neutron Capture in Fissile Material.

Table I lists the average numbers of neutrons released in various fissile materials. In this table, the differences between  $\nu$  and  $\eta$  (defined therein) arises because neutrons are sometimes captured without producing fissioning.

For technical reasons of efficiency and control most nuclear reacting systems operate so that the neutrons which produce the fissioning are “slow”, i.e. have very low kinetic energy. On the other hand, the neutrons which are released in the fission process are “fast” neutrons with relatively high kinetic energy, on the average about 1.5 MeV. Thus they must be slowed down (or moderated) to a low energy. This can be done by elastic scattering of the neutrons from light atoms in a cool moderator. Each scattering reduces the energy of a neutron until its energy approaches the mean energy of the moderator atoms in accordance with the equipartition theorem of statistical physics. Carbon in the form of graphite was used as the moderator in Fermi’s first reactor. Light water ( $\text{H}_2\text{O}$ ) is now commonly used (as in the MIT reactor). Analysis shows that, on the average, one needs about 18 scattering events with hydrogen nuclei (protons) to reduce the neutron energy from 1.5 MeV to a typical thermal energy of 1/40 eV at which point further scattering events can raise as well as lower the neutron energy. The thermal equilibrium is characterized by the physical temperature of the moderator (about 50°C at MIT, but much higher in a power-producing reactor).

The efficiency of neutrons in producing fission depends upon the neutron energy and is conventionally

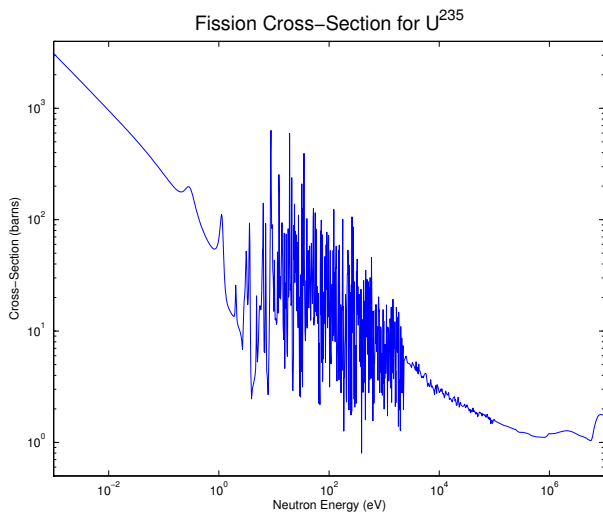


FIG. 1: Schematic Fission Cross-Section for  ${}_{92}^{235}\text{U}$ . Data from atom.kaeri.re.kr/ton.

described in terms of the fission cross section, or effective target area of the fissioning nucleus, expressed in barns (a picturesque name for  $10^{-24}$  cm<sup>2</sup>). The dependence of this upon neutron energy for the case of  ${}_{92}^{235}\text{U}$  is shown in Figure 1 which displays a nice distinction between commonly-designated neutron groups: slow or thermal ( $< 0.1$  eV), resonance (0.1–1000 eV), and fast ( $> 10,000$  eV). Note particularly the much higher fission cross section for thermal neutrons. Neutron physics is sometimes studied in regimes beyond the above classes, in particular as cold or ultra-cold ( $\approx 10^{-7}$  eV). Ultra-cold neutrons (UCN) exhibit very interesting properties. For example, they cannot penetrate surfaces and can be contained in a “bottle”!

An important quantity for reactor design purposes is the fission cross section at the thermal energy which is attained by most of the neutrons after moderation. For a moderator kept at temperature  $T$  (absolute Kelvin), the thermal energy is  $kT$  and at room temperature this is about 1/40 eV. The cross sections for fissionable nuclei are listed in Table II.

Nuclide	Fission (barns)	Capture (barns)	Capture/Fission ratio
${}_{90}^{232}\text{Th}$	—	7.4	—
${}_{92}^{233}\text{U}$	527	54.	0.102
${}_{92}^{235}\text{U}$	577	106.	0.184
${}_{92}^{238}\text{U}$	—	2.7	—
${}_{94}^{239}\text{Pu}$	742	287.	0.387

TABLE II: Thermal Neutron Cross-Sections for Nuclear Materials.

### 3.1. Design Features of a Nuclear Reactor

In the preceding section, we have surveyed some of the physical concepts and parameters that are of significance in thinking about a nuclear chain reaction. Of course, this is far removed from answering the question, “how to make it work?”. Many different reactor designs have evolved, each one aimed at achieving certain objectives. Research reactors produce radiation, radionuclides or other products useful in scientific and medical studies; power reactors produce energy for practical use; production reactors use excess neutrons to transmute the abundant non-fissionable isotope of uranium,  ${}_{92}^{238}\text{U}$ , into fissionable plutonium,  ${}_{94}^{239}\text{Pu}$  for bombs.

Components of a reactor that are common to all designs include:

1. Fuel elements. Either natural uranium or uranium enriched in the isotope  ${}_{92}^{235}\text{U}$ , usually in the form of uranium oxide or alloyed with aluminum and sealed in aluminum tubes or plates.
2. Moderator. Frequently light or heavy water, but in some cases graphite or beryllium.
3. Thermal heat transfer system. Removes the heat generated by conversion of the kinetic energy of the fission fragments. The latter are entirely retained in the fuel elements.
4. Control elements. Neutron absorbing elements such as cadmium are used to control the neutron flux density and hence the rate of the chain reaction and power output of the reactor.
5. Surrounding radiation shield. Intense neutron and gamma radiation, produced by the fission process and the radioactive decay of fission fragments, must be contained by shielding.

The simplest spatial configuration of these components would be many small fuel elements positioned in a spatial lattice and immersed in a liquid moderator which is circulated through an external heat exchanger to dissipate or utilize the heat generated by the process. To maintain the desired power level thermometers and/or radiation monitors would be connected to servo-mechanisms to adjust automatically the positions of cadmium control rods inserted into the lattice. Details of the particular features of the MIT Reactor will be provided to you at the time of your briefing. Useful references on nuclear engineering and reactors include [2–4].

## 4. EXPERIMENTS

### 4.1. Part I: Study of the Maxwell-Boltzmann Distribution of Neutrons in the Nuclear Reactor

In all of the present experimentation we shall use a pulsed, collimated beam of neutrons emerging from the

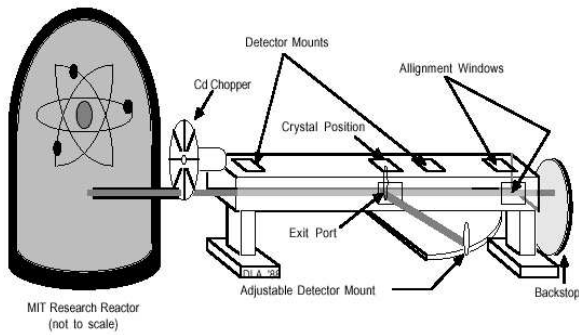


FIG. 2: Experimental setup for time-of-flight spectroscopy at the MIT Nuclear Reactor.

reactor in a setup shown schematically in Figure 2. The distribution in energy of the neutrons in the beam reflects the equilibrium spectrum of the moderated neutrons in the reactor. In accordance with the principles of statistical physics, we anticipate that this spectrum is the Maxwell-Boltzmann spectrum characterized by a temperature that is the same as the physical temperature of the moderating agent in the reactor (normal water in the case of our reactor), providing complete moderation of the neutrons has occurred. Thus we can think of the neutrons in the reactor as constituting a neutron gas in thermal equilibrium with the moderator, with a certain density and temperature. We will examine the velocity spectrum of the neutrons by letting some escape as a collimated beam through a small opening in the reactor shield.

We will measure the velocity spectrum by timing the flight of individual neutrons over a laboratory distance of about 1.5 meters. We do this by “chopping” the beam as it emerges from the reactor to produce periodic short bursts of neutron intensity. After traveling the flight distance the neutrons are detected with a small neutron counting tube, and the occurrence times of the individual counting pulses relative to the starting time of the burst are recorded with a multichannel scaling (MCS) card.

#### 4.2. The Neutron Chopper

The chopper is a slotted disk of neutron-absorbing cadmium which rotates about an axis above and parallel to the neutron beam line, as illustrated in Figure 3. Cadmium is very absorptive to neutrons of energy less than about 0.40 eV (speed of 8760 m/sec), and serves as a good shutter for thermal neutrons. The cadmium disk of thickness 1 mm is sandwiched between two aluminum disks for mechanical stability. Around the periphery of the disk assembly, eight radial slots have been cut in the disk assembly. The width of each slot is 0.95 mm. Immediately in front of the chopper disk (upstream) is a fixed slit opening in neutron absorbing material (boron

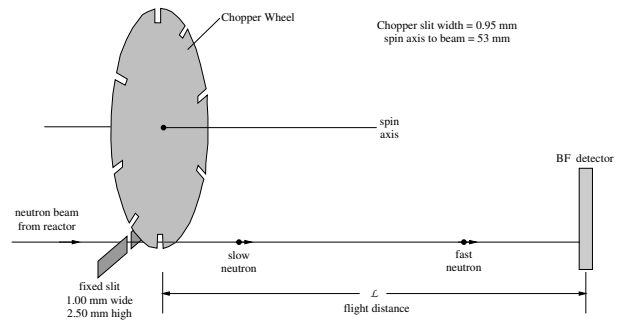


FIG. 3: Schematic diagram of the time of flight spectrometer showing the beam chopper and the  $\text{BF}_3$  detector.

containing plastic) of width 1.00 mm and height 2.5 mm. This serves to define the beam size entering the chopper assembly. The axis of rotation is located 53 mm above the geometrical center of the defined neutron beam. A small speed-controlled synchronous motor rotates the disk. Every time a radial slit passes the fixed slit a burst of neutrons is admitted to the flight line. Since the slit widths are nearly equal the time structure of intensity in this burst (which may contain several hundred neutrons) is triangular, with a full width at half maximum (FWHM) determined by the slit width and rotational speed. You should convince yourself of this feature. Also, consider what it would be for the case of unequal slits.

The rotational speed of the synchronous driving motor is fixed by the power line frequency and is seen as a digital display of the rotational speed in RPM or the neutron burst repetition rate in Hertz. This frequency will be 240 Hz throughout the experiment.

It is necessary to establish a reference time for the origin of each of the neutron bursts. This is done by the periodic interruption of a light beam passing parallel to the neutron beam line between a tiny photodiode and photodetector which is positioned about  $90^\circ$  around the disk from the neutron beam. The geometry is arranged so that a light signal occurs a short time before each neutron burst. The light signal sets the time origin of the MCS used to measure the neutron flight time. Thus the actual neutron burst origin time is slightly later than the MCS origin time by a certain fixed delay which must be determined as a part of the experiment.

#### 4.3. The Neutron Detector

Small gas proportional counters are used as neutron detectors. For this part of the experiment, the counter of choice contains  $\text{BF}_3$  gas in a sealed aluminum tube of diameter 0.5 inch and length 3 inches. High voltage (**bias the  $\text{BF}_3$  detector at +1000 VDC and the  $\text{He-3}$  detector at +1600 VDC**) is applied between the metal tube and a fine center wire. The resulting electric field collects the charges produced by gas ionization caused by the energetic nuclei from the reaction  ${}^1_0n + {}^{10}_5B \rightarrow {}^7_3\text{Li}$

$Li + \frac{4}{2} He$ . The  ${}^{10}_5B$  isotope forming 18.8% of natural boron captures neutrons with a large cross section that varies as  $1/v$ , where  $v$  is the neutron speed. Many nuclei, such as  ${}^1_1H$ ,  ${}^6_3Li$ ,  ${}^3_2He$ , and  ${}^{197}_{79}Au$  exhibit this “ $1/v$  law” capture of slow neutrons (see the plot of the  ${}^{235}_{92}U$  fission cross section in Figure 1).

Our counter contains  $BF_3$  gas at a pressure of 40 cm Hg; a typical neutron passing along a diameter will be detected with an efficiency of about 1%. It is purposely selected to be “thin” (low efficiency) so that a simple analytical correction can be applied in the analysis of the spectral data. Electrical pulses from the counter are amplified in a preamplifier and in a main-line amplifier, selected by a single channel “window” analyzer, and counted by a scaler. Thereafter they are sent to an oscilloscope for observation, and to a MCS for arrival time sorting. The output pulses from the amplifier are about  $5 \mu s$  in duration. Operating details concerning the counter high-voltage, amplifier settings and MCS operating conditions are posted at the experiment location.

#### 4.4. Thermal Spectrum Theory

The Maxwell-Boltzmann (M-B) distribution law describes the distribution in speed (or kinetic energy or momentum) of atoms in a gas in a state of thermal equilibrium. Neutrons within the reactor can be expected to obey a similar distribution law, namely

$$n(v)dv = \frac{4N}{\sqrt{\pi}} \left( \frac{v^2}{v_0^3} \right) \exp\left(-\frac{v^2}{v_0^2}\right) dv, \quad (2)$$

where  $v$  is the neutron speed (m/sec),  $v_0$  is the most probable speed (i.e. the peak of the speed spectrum),  $N$  is volume density of all neutrons (neutrons/m<sup>3</sup>),  $n(v)dv$  is the neutron density for those with speeds falling in the speed interval between  $v$  and  $v + dv$  (see texts on gas kinetic theory, e.g. Reference [5, 6]).

This can be recast in terms of other kinetic parameters such as kinetic energy  $E$  for which we have

$$E = \frac{1}{2}mv^2 \quad \text{and} \quad dE = mv dv, \quad (3)$$

yielding

$$n(E)dE \propto \left( \frac{E}{E_0} \right)^{1/2} \exp\left(-\frac{E}{E_0}\right) dE, \quad (4)$$

with

$$E_0 = \frac{1}{2}mv_0^2 = kT, \quad (5)$$

where  $m$  is the neutron mass.

The corresponding flux density in the collimated beam, i.e. the number of neutrons per unit area per unit time with velocity between  $v$  and  $v + dv$  passing a given point,

is

$$\begin{aligned} j(v)dv &= vn(v)dv \\ &= J_0 v^3 \exp\left(-\frac{v^2}{v_0^2}\right) dv. \end{aligned} \quad (6)$$

As mentioned above, the neutron detector is a “thin” counter for which the efficiency  $e$  varies with neutron speed as  $1/v$ . Thus

$$e = A(1/v), \quad (7)$$

with  $A$  = some constant. If we now call  $j'(v)dv$  the number of detected neutrons per unit area of detector per unit time with velocity between  $v$  and  $v + dv$ , then

$$j'(v)dv = Bv^2 \exp\left(-\frac{v^2}{v_0^2}\right) dv, \quad (8)$$

with  $B$  is a constant. Can you figure out the reason for using a “thin” counter rather than using one with higher efficiency of say 50%, aside from the fact that we don’t need the higher efficiency because the measured intensity is adequately high?

The quantity actually measured by the apparatus in each event is the time interval between the fiducial signal from the photodetector and the detection of a neutron by the  $BF_3$  counter (rather than the velocity). The accumulated data in the MCS is the number  $N_i$  of neutrons detected in the  $i$ -th MCS-time channel corresponding, after appropriate calibration and zero-time correction, to a flight time  $t_i$ . Since  $L = vt$ , we have

$$N_i = D \left( \frac{1}{t_i^4} \right) \exp\left(-\frac{L^2}{v_0^2 t_i^2}\right) \Delta t, \quad (9)$$

where  $\Delta t$  is the finite and constant width of the MCS-time channels, and  $t_i$  is a flight time within the  $i$ -th interval, and  $D$  is a constant.

We note that

$$\ln(t_i^4 N_i) = -\left(\frac{L}{v_0}\right)^2 \left(\frac{1}{t_i}\right)^2 + \text{constant}, \quad (10)$$

or, equivalently, that

$$\ln\left(\frac{N_i}{v_i^4}\right) = Q - \frac{v_i^2}{v_0^2}, \quad (11)$$

where  $Q$  is a constant. Thus a display of the quantity  $(N_i/v_i^4)$  against  $v_i^2$  on semi-log graph paper should be a straight line with negative slope  $(1/v_0^2)$ . It will be convenient to display the data in this way to check the validity of the Maxwell-Boltzmann distribution and to evaluate  $v_0$  and  $T$ .

#### 4.5. Experiment Procedure—Part I

1. Examine the apparatus and, with the aid of an instructor, identify the components and their functions.

2. Activate the chopper motor and wait until it settles to the rotational speed corresponding to a neutron burst frequency of 240 Hz.
3. Place the BF<sub>3</sub> counter (already mounted in a small shield box) at the location point very close to the chopper and set the counter voltage and amplifier conditions at the prescribed levels. Instructions for this will be posted locally.
4. Open the shutter to admit the neutron beam to the apparatus—a yellow “beam-condition” warning light will be activated. As noted previously, the neutron beam is contained in a long square-shaped channel until it is finally absorbed in a shield cage at the end of the flight path. **It is of high intensity and exposure of any part of the body to it must be avoided.** In addition to the thermal neutrons used in this experiment, there are also gamma-rays and unmoderated fast neutrons which are damaging to tissue.
5. Examine the neutron detection pulses from the amplifier on the oscilloscope screen, noting their time width.
6. The Multi-Channel Scaler (MCS) that you will be using is a board plugged into the PC. The presets should be set as follows:
  - a) Dwell time 2  $\mu$ s
  - b) Pass Length 1000
  - c) Pass Count 432,000

The dwell time (s ch<sup>-1</sup>) multiplied by the pass length (ch) must be less than the time interval between consecutive neutron bursts (see note 2 above). Instructions for using the MCS software can be found on-line from the “Help” Menu and in the software the manual in the top desk drawer. Don’t forget to EXPORT the data files into a text readable format after saving them to the default Perkin Elmer format. This latter format is not readable from computers that do not have the MCS software installed.

7. Set the MCS into operation and note the build-up of neutron counts in early time channels of the MCS time display. Since the flight distance is so small (only about 5 cm), neutrons of different speed do not have a chance to spread apart before detection. Collect data over a recorded time interval, stop the collection, and save the data to a file in your personal directory. Only a short collection time will be needed for this, as you see the quick build-up on the MCS display.
8. While you have the counter at the front position just behind the chopper, you can measure the intensity of the beam coming through the stopped, open slit. From this intensity and the known geometry of the collimator tube in the reactor shield, you

can calculate an approximate value for the neutron flux inside the reactor. With the chopper stopped, adjust its angular position to get the maximum intensity as seen in the 5-second counting intervals on the scaler digital display. Record a number of these counts for averaging. Do the same with the chopper oriented so the beam is obstructed by the cadmium in the chopper. The difference between these average values divided by the detector efficiency gives the thermal neutron intensity expressed in neutrons per second. Using the formulae given in Appendix B., along with the known geometrical factors, you can calculate the neutron flux and the neutron density inside the reactor.

9. Move the BF<sub>3</sub> counter to the back position along the flight channel. Again, note the build-up of neutron counts on the MCS display. Neutrons are now found in later time channels distributed over a time spectrum. Collect data for a recorded time interval. This will take about 30 minutes to get statistically meaningful numbers because the neutron counts are now spread over many channels. (The electronic cut-off of high channels is purposely introduced to eliminate overlap from one burst to another.)
10. Close the neutron beam shutter. Measure the distance from the cadmium in the chopper disk to the counter tube center for both positions. Always take these measurements in centimeters with an accuracy to about one millimeter. Record this measurements along with rotational speed, the MCS channel width, and the collection time. Double check your distance measurements, since an error here will affect all of your later analysis.

#### 4.6. Data Analysis

The procedures detailed in this section are readily accomplished using Matlab on the MIT Server or some other mathematical package of your choice.

- 1) Plot your data for the small distance case, neutron counts vs. channel number, and determine the center position and uncertainty. Is the shape what you expect, and does the FWHM agree with what you calculate? Remember that the neutrons have had little chance to spread out. On the other hand, the finite flight time over your small distance has shifted this peak by a small amount relative to the neutron burst origin time. You can correct for this shift by making use of the observed travel time of the peak in the MCS display for neutrons going from  $L_1$  (the short flight distance) to  $L_2$  (the long flight distance). Thus the correction is

$$\frac{L_1}{(L_2 - L_1)}(C_{2p} - C_{1p}), \quad (12)$$

and the neutron time origin channel  $C_0$  becomes

$$C_0 = C_{1p} - \frac{L_1}{(L_2 - L_1)}(C_{2p} - C_{1p}). \quad (13)$$

Here,  $C_{1p}$  is the MCS channel of the center of the approximately triangular distribution obtained when the detector is at the near position;  $C_{2p}$  is the MCS channel position for the peak of the distribution recorded when the detector is at the far position which is at a distance  $L_2$  and correspondingly for  $C_{1p}$ . It is interesting to note that the speed of the neutrons in the peak in the MCS time distribution

$$N_i = C \left( \frac{1}{t_i^4} \right) \exp \left( -\frac{L^2}{v_0^2 t_i^2} \right) \Delta t, \quad (14)$$

becomes  $\sqrt{2}v_0$ , as you can establish by setting its time derivative to zero, thereby obtaining  $t_{\text{peak}}$ , and looking at this dependence on  $L$ . This can be compared to the peak in the velocity distribution which is  $v_0$ .

Note that the channel spread about the peak centered at  $C_0$  (in the data taken at the small distance position) is a direct representation of the time resolution of the system. All later measurements are smeared by this limiting time resolution.

2) Plot a spectrum of your data as taken at the back counter position. Identify on your graph the neutron origin channel position  $C_0$ —all flight times are now established relative to this.

Create a plot of all the data points and an interpolated line. We expect that the spectrum will approach equal asymptotic levels at the two extremes of the spectrum, and that this is a background level by which all observed spectral intensity values should be corrected. Are the deviations of individual points from your smooth curve meaningful on statistical grounds? Remember that the collection of  $N$  statistically distributed events in a measurement means that there is 68% probability that the value  $N$  will fall within  $\langle N \rangle$  of the true value as established by many repetitive measurements.

Since the expected M-B spectrum approaches zero asymptotically at both extremes of the spectrum (because of the  $t^{-4}$  dependence at the high channel (low energy) end and the exponential dependence at the low channel end), the residual or base level that is observed represents a background intensity level arising from leakage neutron events not associated with opening or closing the chopper. Thus all observed intensities should be corrected by subtracting this background level. In assessing this background level for your data, you should note that  $t \rightarrow 0$  for channels just above  $C_0$  so the intensity level for channels just above  $C_0$  should represent the base level. On the other hand, at the other extreme, near the electronic cut-off level of about channel 1000 (or whatever the number of channels has been set to in the MCS software), the M-B spectrum has not completely collapsed to

zero and the observed intensity may be somewhat higher than it would be for even lower channels. We can correct for this residual M-B intensity in high channels by noting that its value, relative to the peak intensity depends upon  $v_0$ . **Previous experimentation has determined  $v_0$ , and calculation has shown that the ratio of this residual intensity in channels above 950 to that at the peak is 0.013.** Using this ratio value, determine the background base value which is most consistent with the observed intensity pattern at both ends of the spectrum. Pay no attention to intensity values corresponding to negative channel numbers (below  $C_0$ ) since they are associated with transparency of the Cd in the chopper and with other leakage neutrons.

3) Create data vectors of  $N_{\text{observed}} - N_{\text{base level}}$  and corresponding  $C_{\text{observed channel}} - C_0$ . Follow with calculated values of the speed  $v$  using your measured flight distance and the individual channel time. Carry a number of significant figures that is consistent with the measurement precision.

Finally, tabulate values of  $N_{\text{corrected}}/v^4$  and  $v^2$ . Make a semi-log plot covering about 3 log cycles of these quantities. According to our M-B theory, these points should fall on a straight line whose slope is  $1/v_0^2$ . Graphical trick: to make full use of 3-cycle log paper, adjust your intensity data by an arbitrary multiplicative factor—this will not affect the slope.

4) You will probably find that the high-velocity data points ( $> 5000$  m/sec) in this semi-log display fall above a straight line fitted to the low-velocity data. Two effects contribute to such discrepancies: (a) The finite duration of the pulses of neutrons that emerge from the chopper causes a smearing of the observed velocity distribution so that it differs significantly from the true flight time distribution (see if you can estimate the effect of this on your data); (b) High energy neutrons generated in the fission process and encountering the relatively cold moderator, are continually diffusing in “velocity space” toward lower velocity with the diffusion driven by an excess at high velocities over the equilibrium Maxwell-Boltzmann distribution.

Deviations from linearity of the plot may also occur at low velocities ( $< 1000$  m/sec) for various reasons such as the high absorption cross sections of reactor materials for slow neutrons. It must be recognized, also, that the background intensity makes up a larger portion of the observed counting rates at the low and high-velocity ends of the data.

In any event, when fitting a straight line to the data, remember both effects and pay special attention to the main center region of the range. Since your physical judgment must establish the range of linearity, it is hardly worthwhile to use a least-squares fitting of the points to a straight line. Use your best judgment in this and es-

timate the uncertainty in the slope of the line. Don't hesitate to calculate values and plot additional points beyond your initial sampling of your smoothed spectral curve in assessing the best line fit. If you find gaps in your selected point distribution, analyze additional intermediate ones which will help in recognizing the linear range.

5) Evaluate the slope of your best straight line (be very careful in this—students frequently have much trouble with the slope of a line on semi-log display) and calculate  $v_0$ ,  $E_0 = 1/2mv_0^2$ , and  $T$  from  $kT = 1/2mv_0^2$ , and justify this relation. Recall in gases  $E_{\text{kinetic}} = \frac{3}{2}m\bar{v}^2$ . Does your neutron temperature  $T$  agree with that of the moderator? Does the peak position in the observed spectrum agree with that expected from your fitted parameters? From the uncertainty in the slope of the line, what are the uncertainties in these quantities?

6) Calculate the neutron flux and neutron density in the reactor from your data obtained in section 4.5 step 7 and the analysis in Appendix B.. If we think of these neutrons as being confined in a walled container, what pressure would they exert on the walls?

#### 4.7. Part II: Bragg Diffraction of Neutrons and the De Broglie Relation [7]

In the early years of this century, physicists were faced with the wave-particle dilemma in describing the properties of the electromagnetic field and how it interacts with matter. Young's interference experiments with visible light (1801), Hertz's experiments with radio waves (1887), and von Laue's discovery of X-ray diffraction (1912) showed wave interference and provided measures of wavelength for electromagnetic radiation from radio to X-rays. On the other hand, Planck's theory of the black-body spectrum (1901), and Einstein's theory of the photoelectric effect (1905) showed that electromagnetic radiation is *absorbed* at a surface in discrete amounts of energy (quanta) and not as a continuous flow. Bohr's theory of the hydrogen atom (1913) showed that electromagnetic energy is *emitted* in discrete quanta. And, finally, Compton's interpretation of his own experiments on the incoherent scattering of X-rays (1923) showed that X-rays of wavelength  $\lambda$  interact with free electrons like particles with energy  $hc/\lambda$  and momentum  $h/\lambda$ . A composite picture was thus formed in which electromagnetic radiation is characterized by the seemingly contradictory concepts of wave frequency and wavelength, and particle momentum and energy.

Recognizing this interrelation for photons between wave and dynamical properties, De Broglie suggested in 1924 (in his PhD thesis) that similar properties should characterize all particles of matter. At that period, matter was considered to be made up of electrons and protons. This meant that electrons and protons (or any composite of them like an atom, a baseball or the earth)

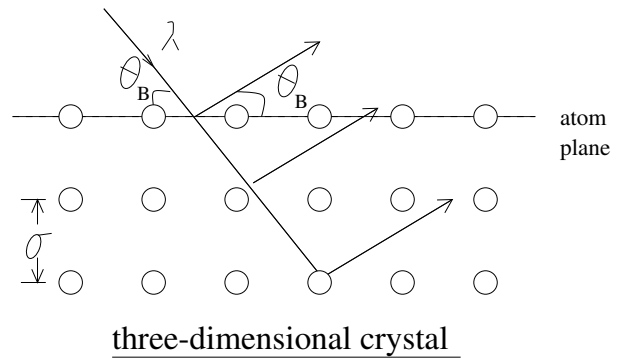


FIG. 4: Schematic representation of a crystal with rows of atoms extending into the page.

in motion should possess a wave character. De Broglie proposed a relation between the wavelength ( $\lambda$ ) and momentum ( $mv$ ):

$$\lambda = \frac{h}{mv}, \quad (15)$$

where  $h$  is Planck's constant. This relation is the same as for photons, with, however, the recognition that photon momentum  $p = E/c$  (with the photon energy  $E = h\nu$  and  $\nu$  the wave frequency of the electromagnetic photon).

Although not taken too seriously at first (it is reported that Einstein himself was incredulous initially), De Broglie's suggestion was given full acceptance with the discovery of electron diffraction by G. P. Thompson and by Davison and Germer in 1927. They drew upon the fact that atoms in a crystal are positioned relative to each other in a very regular way, and that their spacing is a few Angstroms ( $1\text{\AA} = 10^{-10}\text{ m}$ ) in scale. Their experiments on the reflection of electron beams from metal crystals demonstrated that wave interference effects were obtained with electrons of an energy such that their De Broglie wavelength is comparable to the separation of the crystal planes, a result completely analogous to that previously observed with X-ray photons (which certainly were endowed with a wavelength) and interpreted by Laue and Bragg. Since that time, further confirmation of the wave-particle duality has come for other types of particles (waves) such as alpha particles, atoms, neutrons and mesons. We shall see this duality in full display in Part II of this experiment, where we shall again directly measure the velocity of a group of neutrons and at the same time observe the diffraction of these same neutrons by a crystal, thereby establishing their De Broglie wavelength.

We shall first need to know some things about crystals and the wave interference effects that may be observed with them. As mentioned above, a crystal represents a collection of many atoms bound together by inter-atomic forces to form a three-dimensional solid (however, two-dimensional cases and liquid crystals are known to exist). In a perfect crystal, the atoms are positioned in a spatial array (or lattice) with precision, this being determined

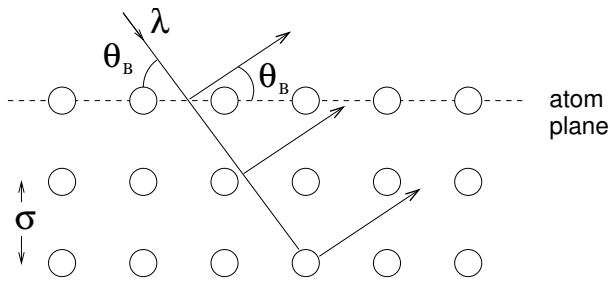


FIG. 5: Schematic representation of a diffraction grating as a one-dimensional set of scattering centers.

by the symmetry and balancing of inter-atomic forces on each atom. With this regularity of position, illustrated schematically in Figure 4, it is easy to envision the overall crystal as being made up of parallel sheets (or planes) of atoms which can serve to provide wave interference between the components of radiation scattered by individual atoms. Almost any textbook on general or modern physics (e.g., reference [8, 9]) will have an elementary derivation of the conditions necessary for constructive interference of radiation scattered from atoms in a crystal plane. These conditions are expressed by Bragg's Law,

$$n\lambda = 2d \sin \theta_B, \quad (16)$$

where  $n$  = order of diffraction (1, 2, 3, ...),  $\lambda$  is the wavelength,  $d$  is the interplanar spacing, and  $\theta_B$ , called the Bragg angle, is the grazing angle of incidence and reflection. It is deceptively similar in appearance to the law describing constructive interference from a one-dimensional set of scattering centers (e.g. a grating), and it is worth pointing out the difference.

In the one-dimensional case, illustrated in Figure 5, the approach angle  $\theta_1$  may have any value, and the exiting angle  $\theta_2$  for constructive interference is then defined by the interference equation with  $\theta_2$  not necessarily equal to  $\theta_1$ . For reasons not so obvious, this generality is not present in three-dimensional diffraction where  $\theta_1 = \theta_2 = \theta_B$ . In fact, diffraction from a crystal always occurs in symmetrical fashion from atom planes with both incident and emergent angles being equal to  $\theta_B$ . (This subtle distinction is discussed in [10] and in various texts on crystallography, e.g., *X-Ray Crystallography*, M. Wolfson, Cambridge 1970.) A given set of atom planes of spacing  $d$  will reflect radiation of wavelength  $\lambda$  with intensity concentrated in a narrow range of angles (typically within  $10^{-5}$  radians) with a maximum at the Bragg angle  $\theta_B$  defined above. This is not true for the one-dimensional grating where, for any incident angle  $\theta_1$ , diffraction maxima occur at angles  $\theta_2$  given by the formula in the figure, provided  $d > \lambda$ .

A crystal may be considered as being made up of an infinite number of different atom plane layers, each set with a different interplanar spacing and different orientation. Bragg diffraction can occur from any of these sets as long as the Bragg Law is satisfied. What we need

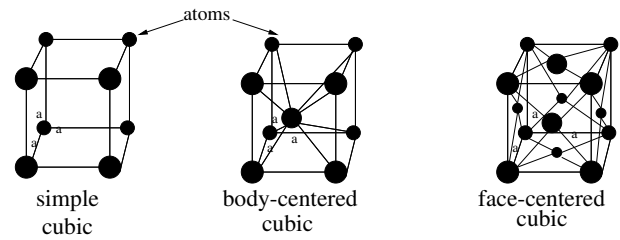


FIG. 6: The three forms of cubic crystals.

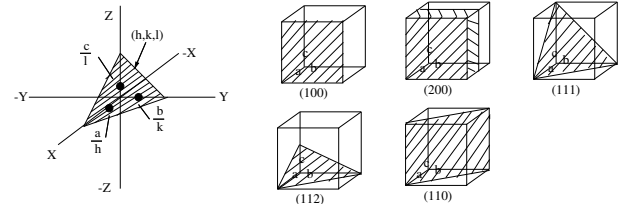


FIG. 7: Diagrams showing how Miller indices are used to define crystal planes.

at this point is a shorthand method of classifying these different sets of planes, which we now develop. Since nature causes atoms to pack together in different ways (but always in a given way for a given species of atoms or molecules; a change of external conditions such as the temperature, pressure, or magnetic field application can invoke a change of structure, a phase transition), it is apparent that many different forms of crystal structure may be encountered. These are classified according to symmetry characteristics: cubic, hexagonal, ortho-rhombic, etc. Common to all forms is the concept of the unit cell which represents the smallest collection of atoms (or molecules) which, when repeated along the three axes, make up the whole crystal. Thus cubic crystals have cubic unit cells and the size of the unit cell  $a_0$  is set by one dimension. However, cubic cells may contain any one of three different atom configurations as shown in Figure 6.

For the general case, the unit cell can be defined by three vectors  $a$ ,  $b$ , and  $c$  directed parallel to the unit cell edges and of magnitude equal to the size in that direction. Furthermore, we can identify the orientation of any plane of atoms in the crystal by the intersections of this plane with the three axes of the unit cell. It is a great convenience to do this in terms of the Miller indices  $h$ ,  $k$ , and  $l$  (small integers) with  $a/h$ ,  $b/k$ ,  $c/l$  being the intersection points of the plane with the respective axes, as illustrated in Figure 7.

We label a particular set of atomic planes as being  $(hkl)$  planes according to these Miller indices. A little geometry will show, for the case of a cubic crystal, that the interplanar spacing  $d_{hkl}$  will be given simply by

$$d_{hkl} = \frac{a_0}{(h^2 + k^2 + l^2)^{1/2}}. \quad (17)$$

In our experiment, we shall be using a metal crystal of pure copper which has a face centered cubic structure (four unique atoms per unit cell) with unit cell size

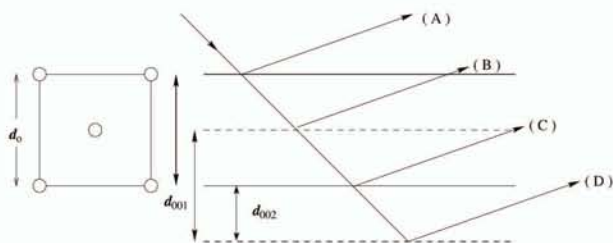


FIG. 8: Illustration of Bragg reflection from a fcc crystal in which destructive interference between reflections from adjacent (001) planes occurs.

$a_0 = 3.6147 \text{ \AA}$ . Note that this value of  $a_0$  may be calculated from the measured density  $\rho = 8.939 \text{ gcm}^{-3}$ , Avogadro's number  $6.0221 \times 10^{23}$  atoms per mole, the molecular weight  $63.57 \text{ gXF}$ , and the number of atoms per unit cell. Check that this is so. Also calculate interplanar spacing values for planes (200), (220), and (111) which you will be using in the experiment. You should identify, in the above figure of cubic unit cells, just which atoms are unique to the unit cell—there are four for face centered cubic (how many are there for the other cells?). Incidentally, among some common elements, Fe, Cr, Na, and Mo crystallize as body centered cubic (bcc) and Cu, Al, Au, and Pb as face centered cubic (fcc). No element is known to exist in simple cubic form.

Before leaving our crystallographic considerations, we should investigate whether there are restrictions on the appearance of Bragg diffraction from the many ( $hkl$ ) sets of planes. To illustrate this for our fcc case, a view of the unit cell normal to a face shows atoms and atom planes as shown in Figure 8. There are sheets of atoms separated by the fundamental distance  $d(002) = a_0/2$ , with common atomic density in all sheets. If we were to attempt to observe (001) diffraction as prescribed by Bragg's Law, we would find reflected rays (A) and (C) to be in phase, as would (B) and (D), but the two groups would be out of phase with respect to each other, and hence overall destructive interference would occur. Thus zero intensity in (001) diffraction is expected, but finite intensity in (002) diffraction. Without going into detail, **the general rule for an fcc structure is that the Miller indices must be either all even integers or all odd integers in order for constructive interference to occur.** Thus there will be no (100), (110), (221) diffraction occurring, but there can be (020), (111), (022), (311) for fcc. Other crystal structures would have different selection rules. Miller indices can be taken negative as well as positive, and a negative index is written as a bar over the index. Thus  $(1\bar{1}\bar{1})$  would designate an allowed set of planes in the fcc structure Bragg diffraction.

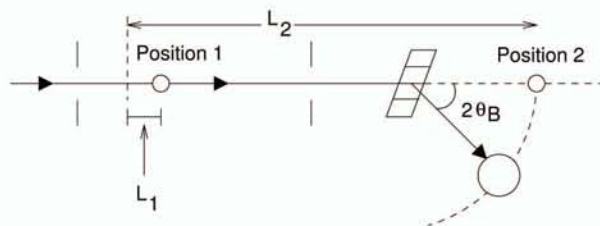


FIG. 9: Schematic diagram of the neutron beam diffracted from the copper crystal.

#### 4.8. Experiment Arrangement and Procedure

We shall use the same neutron beam as in Part I. As we have seen, it is a full spectrum beam with all neutron speeds (or as De Broglie asserted, all wavelengths). However, before detecting it on its normal straight flight line, we shall interrupt it with a diffracting crystal of copper. After repositioning the detector, we can detect the Bragg diffracted beam in the direction that makes an angle of  $2\theta_B$  with the incident beam, as shown in Figure 9.

The copper crystal will be positioned along the neutron flight line, somewhat in front of the position where you placed the detector for Part I spectrum measurement. Notice that there is a fixed slit opening (of width 3.0 mm) just before (upstream from) the crystal position, and this serves to further define the direction of neutron ray trajectories (along with the fixed slit in front of the chopper disk shown in Figure 3) that can hit the crystal. It was there during your spectrum measurement, but served no particular purpose, since we were interested only in flight distance to the detector and not the direction of rays.

If a particular set of crystal planes ( $hkl$ ) is oriented at an angle  $\theta_B$  from the incident beam direction, neutrons with wavelengths in a narrow band will satisfy Bragg's Law and hence be diffracted at angles in a narrow range around  $2\theta_B$  from the incident beam direction. We can detect this diffracted beam by placing our detecting counter at the appropriate angular position. In our experiment, we shall select various orientation positions of the crystal (thereby selecting  $\theta_B$ ) and simultaneously measure the flight time of the diffracted neutrons which arrive at the detector. This provides both the wavelength  $\lambda$  (from the Bragg Law) and the velocity  $v$  of the diffracted neutrons. By changing the crystal orientation (and the detector position), we can scan over a range of  $\lambda$  and  $v$  and test the De Broglie relation in a very direct way.

*a. 1) The Crystal* The copper crystal has been grown and cut in the form of a small disk of diameter about 15 mm and thickness about 2.3 mm. Copper metal exists usually in polycrystalline form, i.e., it is made up of many microscopic crystallites (perhaps about  $1 \mu\text{m}$  in size) oriented at random. Our single crystal has been prepared in a special way (called the Bridgman method): the metal was melted in a crucible of special shape, and the temperature was very slowly reduced through the freez-

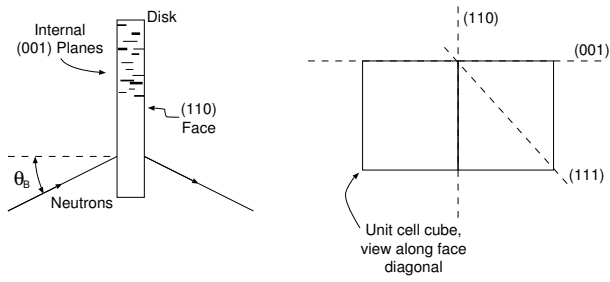


FIG. 10: Illustration of the orientation of the crystal planes in relation to the geometrical shape of the crystal.

ing temperature with a controlled temperature gradient. This permits a single crystal to grow to a size limited only by the crucible dimensions (if the conditions are right!). Our crystal disk has been cut from such a grain after establishment of the grain orientation by diffraction techniques (neutrons, of course!). The flat faces of the disk have been cut and surface polished to high precision—they are parallel to (110) crystallographic planes within 1 arc minute. Looking down on the crystal disk, we see the unit cell as illustrated in Figure 10.

In testing the De Broglie relation, we shall use diffraction from the (002) planes which are accurately perpendicular to the (110) faces. Thus we shall be using the disk in transmission orientation, i.e., the neutrons will pass symmetrically through the disk. Copper is relatively transparent to neutron radiation with an absorption cross section of 3.69 barns for thermal radiation of speed 2200 m/sec. You should calculate the intensity loss this implies.

The crystal disk has been attached to a support plate with our (002) planes vertical, and this in turn is supported by a goniometer, a device for controlling angular orientation. A vernier on the goniometer angle scale permits angular position setting to 0.1 degree around the vertical axis. You will note that the goniometer-crystal assembly is a unit package, which can be attached to the neutron guide channel so that the crystal is automatically positioned in the beam.

*b. 2) Pre-Oriented of Crystal With Laser Beam (Neutron Beam Shutter Closed)* In order to set the crystal diffracting planes at selected Bragg angle positions, we first need to establish the goniometer scale reading at which the crystal planes are parallel to the incident neutron direction. Having done this, the crystal can then be turned and the change in goniometer angle reading will give the angle of incidence of the neutron beam with accuracy.

We shall use a highly collimated laser light beam to do this with the assembly shown in Figure 11. A laser source will be mounted at a right angle to the neutron beam line at the far end of the flight channel. The light beam will be reflected along the axis by a mirror and we want to orient the light beam so that it coincides with the neutron beam that will strike the crystal. By careful

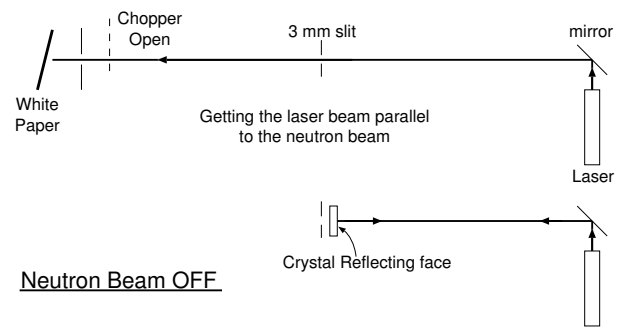


FIG. 11: Arrangement of the apparatus for alignment with a laser. laser.

positioning of the laser and the mirror, you can arrange that the light beam passes through the centers of the two defining fixed slits as well as through one of the slots in the chopper wheel.

- Adjust the mirror or the laser so that the light beam passes through the center of the back fixed slit—you can see the laser beam hitting the chopper wheel.
- Turn the chopper wheel so that the right-left side slots on the wheel are symmetrically positioned relative to the channel—this brings the bottom chopper slot into approximate coincidence with the front fixed slit.
- Realign the mirror-laser so that the light beam passes through the centers of both the back slit and the bottom chopper slot.
- Slide a slip of paper in front of the front fixed slit so that you can see the beam passing through all three slits, and refine the angular position of the wheel to get a maximum light spot intensity on paper—you now have made all three slits collinear.
- Now further align the laser-mirror so that the light beam passes through the centers of the back slit and the bottom chopper slot. Do this with care, and estimate how close in angular orientation you have positioned the laser beam relative to the neutron beam axis. Leave the laser beam undisturbed.

Following this laser beam alignment, the goniometer-crystal assembly is put into position and locked with screws. The crystal now interrupts the laser beam and reflects it back to the laser source. By turning the crystal with the fine goniometer control, the reflected spot is moved on the face of the laser source. Adjust this until the reflected spot is at the same horizontal position as the source spot—a dirty microscope slide is waxed on the front of the laser so that you can see the two spots. In this way, you have arranged that the polished, reflecting surface of the crystal (which is accurately parallel to (110) planes) is perpendicular to the laser beam line

(or the neutron beam line). It follows that the internal (002) planes are parallel to the neutron beam line. Read and record the goniometer angle position with vernier interpolation. Practice with the vernier—always with both you and your partner checking each other. Estimate from the sensitivity of the positioning the accuracy with which you are establishing the zero angle position. All later angle settings are now referred to this value.

c. 3) *The Detector* Instead of using the low efficiency, thin  $\text{BF}_3$  counter that was used in the Part I spectrum measurement, it will be helpful to use a high efficiency (about 90%) counter with  ${}^3_2\text{He}$  gas. This is similar in operation to the  $\text{BF}_3$  counter, but it contains isotopic  ${}^3_2\text{He}$  gas at high pressure, about 40 atmospheres.  ${}^3_2\text{He}$  is the very rare and expensive isotope of elemental helium. As with boron,  ${}^3_2\text{He}$  also exhibits a  $1/v$  absorption cross section for neutrons. The same counting circuit will be used, but different counter voltage and amplifier gain setting will be needed—these conditions will be posted locally.

d. 4) *Crystal Diffraction Measurements*

- a) Set the crystal orientation so that the (002) planes have  $\theta_B = 20^\circ$  as closely as you can read the vernier. Leave the chopper motor off and put the chopper slot in the open position (you would have arranged this in the laser beam prealignment).
- b) Open the neutron beam shutter so that a steady neutron beam falls on the crystal.
- c) Without disturbing the crystal orientation, move the counter in angle position around  $2\theta = 40^\circ$ —there is a crude angle scale on the table and a paper vernier scale on the counter box. With Bragg diffraction occurring at the crystal, we expect a localized intensity peak at about  $40^\circ$  scattering angle. Measure the intensity with short time counting in the electronic scaler at different positions of the detector using steps of  $0.25^\circ$ . Plot this immediately, and determine the center position.
- d) Set the chopper wheel in motion and stabilize at the 240 Hz burst rate as before.
- e) **TIME SAVING HINT: Read Appendix B and do transmission cross-section measurements as part of the next step**
- f) Collect data in the MCS giving the flight time spectrum of the neutrons which are diffracted from the (002) planes in the crystal. There should now be a sharp peak at the flight times of the selected monochromatic neutrons. You may also see a lower intensity peak characteristic of  $\lambda/2$  in second order diffraction from the same planes. Collect enough MCS data for print-out. If you see second order peaks in the MCS display, collect enough data to determine their flight time as well as for the first order.
- g) Repeat for other selected  $\theta_B$  values:  $30^\circ$ ,  $25^\circ$ ,  $20^\circ$ , and  $15^\circ$ . In setting other  $\theta_B$  positions, it is worthwhile to redetermine the counter position as in 4(c) above. An off-center detector will produce an error in the measured speed relative to that expected from the Bragg angle of the crystal. You expect the scattering angle to be close to  $2\theta_B$  in each case. Remember that the  $\theta_B$  value read on the more accurate goniometer is the primary angle quantity and the counter position is not of use in the later analysis. You want only to have the counter in the central part of the diffracted beam. Once you have determined this central part for each angle and measured the spectrum at that angle, you should also take a second spectrum through the boron absorber (pyrex beaker-bottom) for each angle. You will use these data for checking the  $1/v$  dependence of the cross-section for boron in Part II.
- h) At the end of data runs, measure the flight path distance ( $L_1 + L_2$  in Figure 9) of counter center from cadmium chopper wheel; it is different than in Part I. Double-check this measurement.

e. *Analysis of Crystal Data* Graph the time spectrum data obtained at the various  $\theta_B$  selections—only the peaks plus their nearby background are of interest here, including any small  $\lambda/2$  ones. Notice that the channel widths of these are essentially the same as your resolution width determined in Part I. Establish the centers of these peaks (use the steep sides of the peak in this), and correct for the neutron time origin  $C_0$  determined in (h) above.

Calculate the wavelength and corresponding neutron speed (with significant figures consistent with the measurement precision) for the various monochromatic beam observations. Tabulate your data and graph  $v$  vs.  $1/\lambda$  with scales including the origin. According to the De Broglie relation, your data points should fall on a straight line with slope  $h/m$  which passes through the origin. On your graph, draw the expected line using accepted values for  $h$  and  $m$ . This is an ideal case for applying a least-squares treatment of the line fitting (anchor the fitted line at  $v = 0 = 1/\lambda$  since the De Broglie Law requires this).

Analyze the possible contributing errors that enter into your observations and establish the uncertainty in the slope of your linear fit. Is this consistent with the difference between your result and that expected from established constants? Typical runs show agreement to 1.0% or so.

Analyze the  $2\theta$  scans that you made in establishing the centered detector position in the Bragg reflection. Considering the ray geometry falling on the crystal and the angular width of the detector opening, this can tell you something about the perfection of the copper crystal.

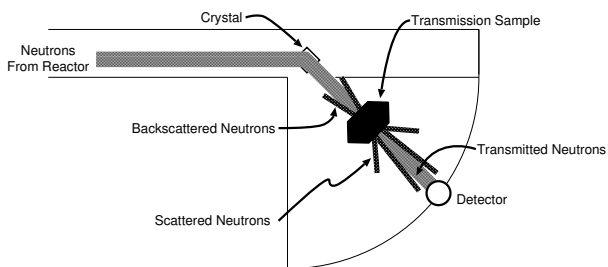


FIG. 12: Plan view of the experimental setup for measuring the attenuation of monoenergetic neutrons in a sample.

#### 4.9. Part III: Additional Crystal Diffraction Observations and Uses of Crystal Monochromated Neutrons

There are a number of other experiments that you can perform with the simple one-axis spectrometer (more elaborate, sophisticated spectrometers sometimes involve three axes of scattering in research studies). You will have time in the scheduling to do at least one of the following. The monochromatic diffracted beams from the copper crystal are of low intensity (unlike the hot, direct white beam), and are safe to experiment with.

#### 4.10. Transmission of Slow Neutrons Through Materials

Most materials are relatively transparent to slow neutrons. This arises because neutrons carry no Coulombic charge (experiments have shown this to be less than  $10^{-22}$  electron charges!), and thus they don't interact with the charge distribution in atoms by means of the long-range Coulombic interaction. They do interact with the nuclei of atoms through the short-range nuclear force interaction, and this is conveniently quantified by a nuclear scattering cross section ( $\sigma_S$ ) and a nuclear absorption cross section ( $\sigma_A$ ). Scattering cross sections do not vary very much from nucleus to nucleus and have values of a few barns ( $10^{-24}$  cm<sup>2</sup>). On the other hand, capture or absorption cross sections vary widely depending upon the distribution of nuclear energy levels and thus nuclear resonance effects may be encountered. In illustration of this, we may note that the absorption cross section of carbon for thermal neutrons is only about 0.0034 barns, whereas for some exotic rare-earth nuclei this becomes as large as several million barns. Absorption cross sections invariably are sensitive to neutron energy (the  $1/v$  law mentioned earlier is a mild example of this) and resonance behavior is not uncommon.

You can study some of these cross sections by using the monochromatic, Bragg diffracted beam from the copper crystal and establishing the transmission ( $T$ ) of a piece of material for this beam, as illustrated in Figure 12.

By definition,

$$T = \frac{I \text{ (intensity passed through the sample)}}{I_0 \text{ (intensity incident on the sample)}}. \quad (18)$$

This can be shown to be

$$T = \frac{I}{I_0} = \exp \left[ - \sum_i M_i \sigma_{iT} \right] \quad (19)$$

with the index  $i$  symbolizing different nuclear species in a composite sample,  $\sigma_{iT}$  the transmission cross section (the sum of both  $\sigma_S$  and  $\sigma_A$ ) per nucleus of the  $i$ -th species, and

$$\begin{aligned} M &= \text{areal density of nuclei} \\ &= \text{number of nuclei/cm}^2 \text{ sample} \\ &= \text{volume density of nuclei} \cdot \text{sample thickness.} \end{aligned}$$

Plate samples of Fe, Al, Cd, and boron-containing Pyrex glass are available for transmission cross section study. For Fe and Al, the transmission is dominated by the scattering process (hence it is relatively insensitive to neutron energy), whereas for Cd and B, absorption dominates with significant dependence upon neutron energy. You will want generally to spend longer periods collecting intensity data through the sample than without...see Appendix A notes on transmission measurements. Study all samples at fixed wavelength corresponding to  $\theta_B = 20^\circ$  and, as well, the boron sample at several wavelengths (energies).

The intensities to be used in obtaining  $T$  are best established from the MCS flight time spectral print-out. By summing the intensity in all channels over the monochromatic peak (corrected for background of course), you obtain the integrated intensity in the Bragg reflection. Normalize these to a common data-collection time interval in getting  $T$ . With the Pyrex plate, the strong absorption cross section of B dominates, and you can establish the  $1/v$  law for this by measuring the transmission over a range of neutron velocities. Established values for the cross sections can be found in Figure ???. Compare these with what you determine from experiment. Perhaps you have something else to place in the neutron beam whose transparency to neutrons you would like to assess. For instance, a thin plate of plastic (containing lots of hydrogen) will attenuate the neutron beam about as much as the thick iron plate!

#### 4.11. Sensing of Bragg Diffraction by Other Crystal Planes

In Part II above, you have seen Bragg diffraction by internal (002) planes which are perpendicular to the major (110) faces of the Cu crystal disk. There are of course many other sets of planes in the crystal that may be used to satisfy Bragg diffraction. You can reorient the crystal

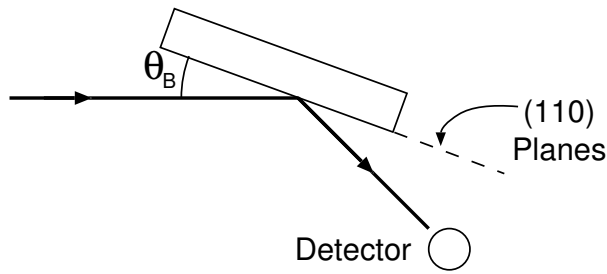


FIG. 13: Reorientation of the crystal to study diffraction from the (220) planes.

disk by turning the goniometer setting through an angle of exactly  $90^\circ$  from your laser beam setting, thereby bringing the (110) faces into coincidence with the neutron beam axis. A further turn will select a Bragg angle for diffraction by the (220) planes (remember that (110) diffraction is forbidden), and from the flight time spectrum yielding  $v$  and  $\lambda$ , you can evaluate  $d_{(220)}$  and see if this is consistent with what is expected.

In a similar manner, you can pick up the (111) planes for diffraction—see earlier crystal sketches to identify where these are located for orientation.

- [1] B. B. Clifford Shull, *Nobel prize lecture*, Nobel Prize Lecture (1994).
- [2] A. Foster and R. Wright, *Basic Nuclear Engineering* (Allyn and Bacon, Boston, MA, 1977), tK9145.F754 ScienceLibrary Stacks.
- [3] A. Henry, *Nuclear Reactor Analysis* (MIT Press, Cambridge, MA, 1975), qC786.5.H46 Science Library Stacks.
- [4] A. Nero, *Guidebook to Nuclear Reactors* (U.C. Press, Berkeley, CA, 1979), tK9202.N45 Science Library Stacks.
- [5] C. Kittel and H. Kroemer, *Thermal Physics* (W.H. Freeman, New York, 1980), qC311.5.K62 Physics Department Reading Room.
- [6] F. Reif, *Fundamentals of Statistical and Thermal Physics* (McGraw-Hill, New York, 1965), qC175.R361 Physics Department Reading Room.
- [7] W. H. Bragg and W. L. Bragg, *Analysis of crystal structure by means of x-rays*, Nobel Prize Lecture (1915).
- [8] P. Tipler, *Foundations of Modern Physics* (Worth Publishers, Inc., 1969), qC21.T595 Science Library Stacks.
- [9] J. McGervey, *Introduction to Modern Physics* (Academic Press, New York, 1971), qC21.2.M145 Physics Department Reading Room.
- [10] B. Rossi, *Optics* (Addison Wesley, Reading, 1957), qC355.R831 Physics Department Reading Room.

#### APPENDIX A: TRANSMISSION CROSS-SECTION MEASUREMENT

As illustrated schematically in Figure 14, one measures the diminution in the beam intensity caused by the insertion of a given absorber between the beam and the detector. The data consist of the total numbers of neutrons detected per unit time,  $N_0$  and  $N$ , integrated over the time-of flight spectrum, with correction for background (baseline), and with and without the sample in the monochromatic neutron beam. One then calculates the transmission  $T$  and finally the effective cross sectional area  $s$  of the scattering-absorption center according to the relation

$$T = \frac{I}{I_0} = \frac{N}{N_0} = e^{-M\sigma} \quad (\text{A1})$$

Question (1): What is the uncertainty  $\Delta\sigma$  in the  $\sigma$  value?

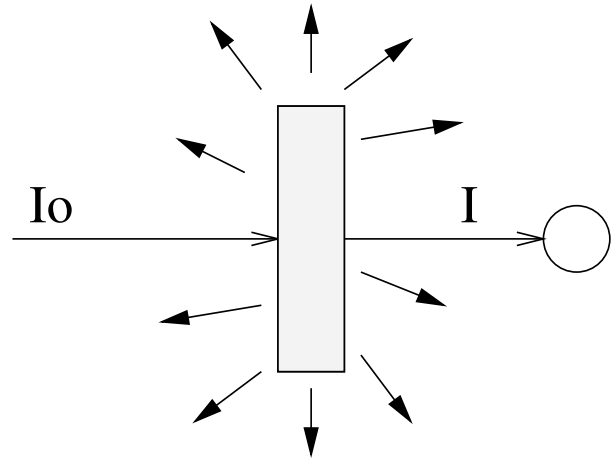


FIG. 14: Schematic diagram of an attenuation measurement.

Answer: From the theory of propagating errors we have the equation

$$\left(\frac{\Delta T}{T}\right)^2 = \left(\frac{\Delta N}{N}\right)^2 + \left(\frac{\Delta N_0}{N_0}\right)^2, \quad (\text{A2})$$

i.e. the fractional error in  $T$  is the square root of the sum of the squares of the fractional errors in the the intensity values. Since  $\Delta N = \sqrt{N}$  for a statistically random collection of  $N$  events, it follows that

$$\frac{\Delta T}{T} = -M\Delta\sigma = \left(\frac{1}{N} + \frac{1}{N_0}\right)^{1/2}. \quad (\text{A3})$$

Question (2): If we want to spend a total collection time  $t_0$  distributed between sample collection time  $t_s$  and incident beam collection time  $t_B$ , what is the optimum distribution of collection time so as to minimize  $\Delta T$  and  $\Delta\sigma$ ?

Answer:  $N_0 = \alpha t_B$  and  $N = T\alpha t_s$ , where  $\alpha$  is the collection rate of incident beam intensity and  $t_s = t_0 - t_B$ . It follows that

$$\frac{\Delta T}{T} = \left(\frac{1}{T\alpha t_s} + \frac{1}{\alpha t_B}\right)^{1/2}. \quad (\text{A4})$$

For minimization of  $\Delta T$ , we want

$$\frac{d(\Delta T)}{dt_B} = 0. \quad (\text{A5})$$

This is satisfied when

$$\frac{1}{T(t_0 - t_B)^2} - \frac{1}{t_B^2} = 0 \quad (\text{A6})$$

(check this out) which, when solved for  $t_B$ , yields the expressions

$$t_B = t_0 \frac{\sqrt{T} - T}{1 - T} \quad \text{and} \quad t_s = t_0 - t_B = t_0 \frac{1}{1 + \sqrt{T}} \quad (\text{A7})$$

and the ratio of collection times

$$t_s/t_B = T^{-1/2}. \quad (\text{A8})$$

Thus for high  $T$  (i.e.  $T \approx 1$ ) we want equal collection times. On the other hand, for small  $T$ , we want to distribute the time so that more time is spent collecting neutrons through the sample. For example, if  $T = 0.1$  for a sample, you will attain highest precision in the calculated value for  $\sigma$  if the sample collection time is about three times longer than the open beam collection time. Of course, increasing the total collection time  $t_0$  also improves the precision. In estimating how you should best distribute the collection time, you can get a preliminary estimate of  $T$  for a sample by looking at the rate of intensity build-up on the MCS scope and comparing this with that obtained with the open beam.

A good sequence procedure for studying the different samples at fixed  $\theta_B = 20^\circ$  position is: (1) Open beam, (2) Al, (3) Fe, (4) B, (5) Cd, and (6) Open beam. Hopefully your start-end ‘‘Open beam’’ results are the same and you can average them. Time all collection runs so that they can be normalized.

In placing samples along the beam line, remember that we do not want to count any of the scattered intensity. This means that we want scattering samples to be well away from the detector so that the detector solid angle as seen from the sample is small compared to total  $4\pi$  steradians.

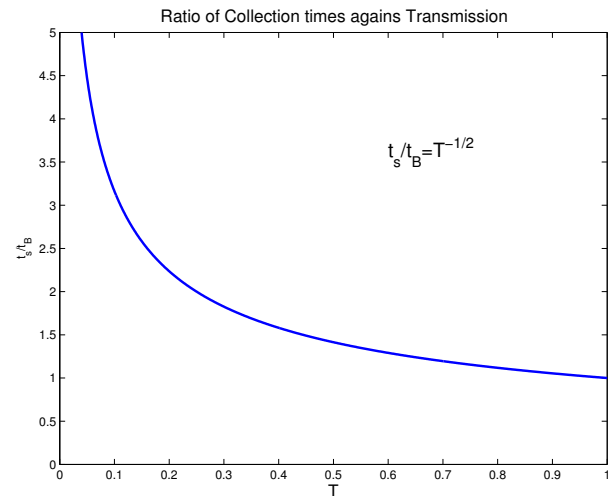


FIG. 15: Plot of the ratio of collection times against transmission.

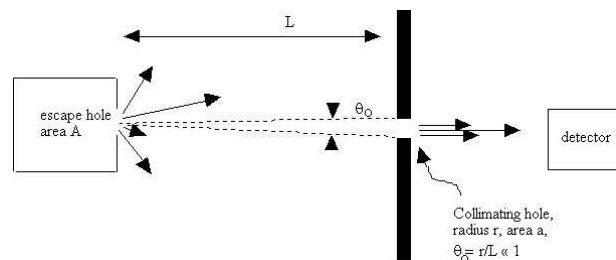


FIG. 16: Schematic of geometry necessary to calculate the neutron flux and neutron density.

## APPENDIX B: CALCULATION OF NEUTRON FLUX AND NEUTRON DENSITY IN REACTOR

The neutron density  $n$  (neutrons  $\text{cm}^{-3}$  irrespective of speed or direction of travel) and the neutron flux  $\phi_0 = nv$  (neutrons  $\text{cm}^{-2}\text{sec}$ ) inside the reactor may be calculated from your intensity measurement obtained in Section 4.5 item 7. We can model this problem as being similar to that found in many textbooks of statistical mechanics or thermodynamics (in particular see Sections 7.9–7.12 in Reference [6]).

Consider a gas of density  $n$  in thermal equilibrium inside a container surrounded by vacuum. A small hole is present in the container wall so that gas atoms of all speeds traveling in all directions escape out through the hole.

An additional collimating hole is placed at a large distance  $L$  from the container wall along a line perpendicular to the container wall so that a collimated beam of atoms of all speeds will pass through the collimating hole and be detected by a detector placed behind the hole. Thus following Reif eq. 7.11.9, the collimated current  $I$  (atoms/second) passing through the collimating hole

would be expressed as

$$\begin{aligned}
 I &= A \int_{v_x > 0} v^3 f(v) dv \int_0^{\theta_0} \sin \theta \cos \theta d\theta \int_0^{2\pi} d\phi \\
 &= \pi A \theta_0^2 \int_0^\infty v^3 f(v) dv \\
 &= \frac{1}{4} A \theta_0^2 n \bar{v} \\
 &= A \frac{a}{4\pi L^2} n \bar{v}, \tag{B1}
 \end{aligned}$$

where as in Reif,  $\bar{v}$  is the average speed of the Maxwell-Boltzmann speed distribution. The average speed is related to our most probable speed  $v_0$  (see Equation 2) as

$$\bar{v} = \frac{2}{\sqrt{\pi}} v_0 \tag{B2}$$

which you have evaluated in the Maxwell-Boltzmann spectrum analysis.

For our neutron case, neutrons are delivered to a low efficiency detector ( $e = 0.010$  averaged over the spectrum) behind the chopper area ( $a = 2.4 \text{ mm}^2$ ) by a long, converging, tapered collimator tube. The dimensions of this collimator tube are such that each point of the exit area sees a source area of  $2.0 \text{ cm}^2$  on the front surface of the oversize insert tube extending through the  $\text{D}_2\text{O}$  reflector to the center line below the reactor volume. The distance from the exit area (the chopper slit) to the front surface source is 310 cm. Using these numerical parameters and your measured intensity you can calculate  $n\bar{v}$  (commonly called the reactor flux) and  $n$ . It is to be recognized that these values are approximate (within a small factor of order unity) because our assembly does not match the features of the model exactly. We do not have a sharp containment wall for the neutrons and the void volume of the insert tube can perturb the local flux. This flux value would scale with the reactor operating power level.

### APPENDIX C: EQUIPMENT LIST

Manufacturer	Description	URL
MIT	Research Reactor	
LND	He-3 Detector	lnd.com
LND	BF <sub>3</sub> Detector	lnd.com
Canberra	Proportional Counter preamp	canberra.com
Canberra	Amplifier	canberra.com
Ortec	Multi-Channel Scaler	ortec-online.com

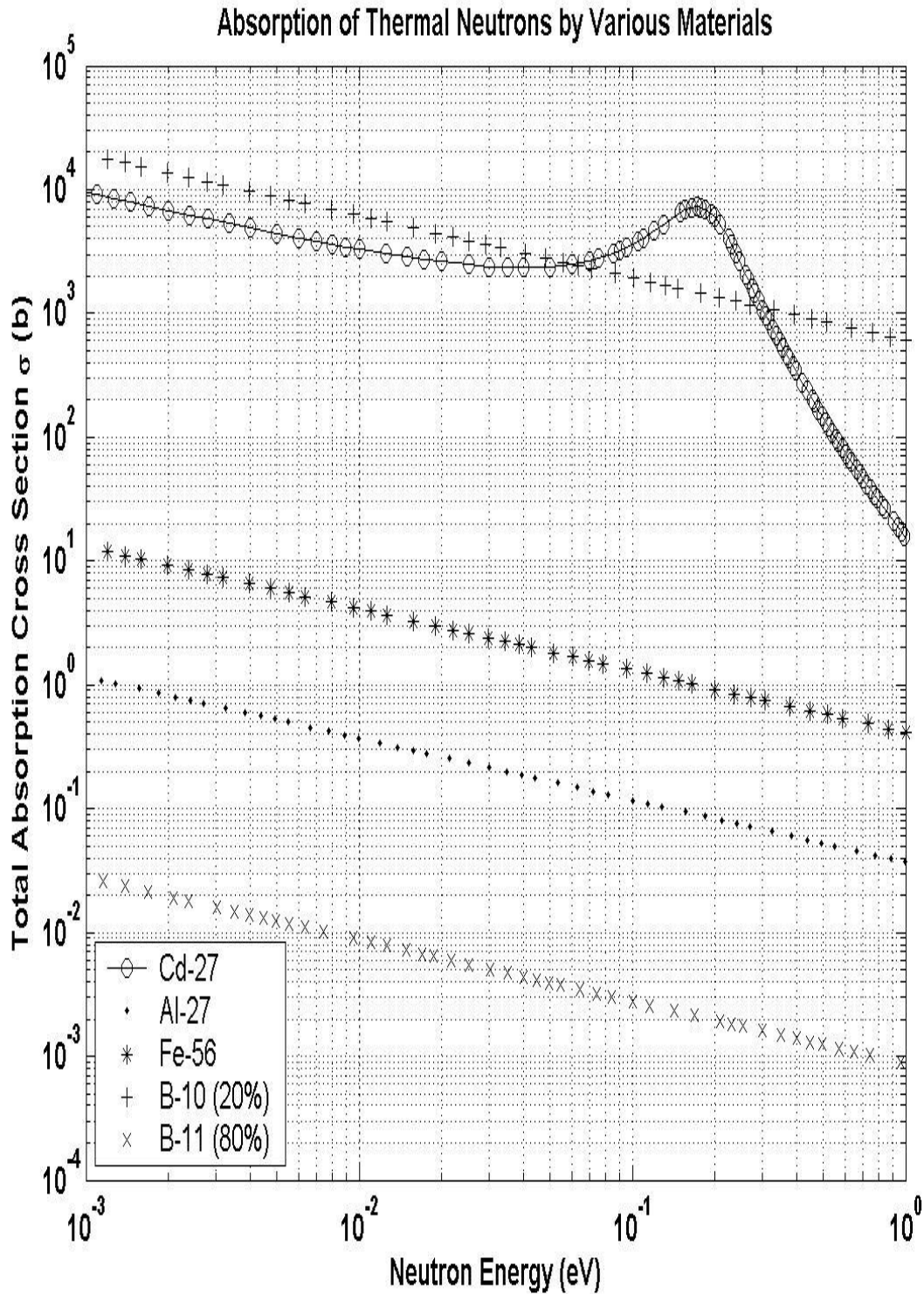


FIG. 17: Total absorption cross-sections for neutrons as a function of energy for B, Cd, Fe, and Al. Data from [atom.kaeri.re.kr/ton](http://atom.kaeri.re.kr/ton). The percentages next to the Boron isotopes indicate their relative natural abundances.